ISABE-2015-20238

3D- MODELLING AND SIMULATION OF THERMODYNAMIC PROCESS AND AEROSOL PRECURSORS TRANSFORMATIONS IN HIGH-PRESSURE TURBINE (HPT) OF AN AIRCRAFT ENGINE WITH DIFFERENT OPERATING CONDITIONS

T.H. Nguyen*, A. Gerboud and F. Garnier
ETS (École de Technologie Supérieure)
1100 Notre-Dame West Street, Montreal, QC H3C 1K3, Canada
* T.H. Nguyen: trung-hieu.nguyen.1@ens.etsmtl.ca

Abstract

In this work, the 3D design of a stator, rotor of a high pressure turbine is performed by using one way coupling between a physicochemical box model and multidimensional Navier-Stokes solver (FLUENT software) method. Various series of three-dimensional calculations including approximately 5,000,000 elements are carried out to calculate aero-thermodynamic fields for a first stage of high-pressure turbine (HPT) of the CFM56 aircraft engine. The results show that the major pollutants of thermodynamic and chemical process are nitrogen NO_x, sulfur oxides SO_x and soot. The phenomena involving the complex interactions between the geometrical parameters, thermodynamic and chemical processes of the aerosol precursor formation in the turbine with different operating conditions are analyzed and investigated.

Keywords: *Aerosols, high-pressure turbine, CFD, chemical pollution, aircraft engine*

1. Introduction

Civil aviation causes to the degradation of air quality around airports (SO_x, NO_x, special hydrocarbons…) and climate change through its greenhouse gases (CO_2, water vapor) emission, as well as particulate matters [1]. These particles include soot particles formed in the combustor, volatile aerosols initiated by gaseous precursors emitted in the post combustor region, downstream of combustor.

Although the aircraft emissions represent today only about 3% of all those produced on the surface of the earth by other anthropogenic sources, they are mostly released in the very sensitive region of the upper troposphere/lower stratosphere. These emissions have a radiative effect reinforced by specific physical and chemical processes at high altitudes, such as cloud formation and ozone production. In this context, most of the work to-date assessed that the actual effect of aviation on the climate could potentially be 2-3 times higher than estimated from the only greenhouse effect of CO_2 emitted. However, these estimates are affected by very large uncertainties, which reach nearly 50% of the values presented in the Intergovernmental Panel on Climate Change (IPCC) reports. These uncertainties are partly due to the lack of knowledge on the thermodynamic process and the mechanisms of production of sulfate and nitrate aerosol precursors in the internal flow of the engine.

Concerning the thermodynamic process, the flow in the aircraft engine is complex. Recent works have addressed this problem but they are mainly based on simplified thermodynamic calculations and numerical calculations 1D or 2D but very little in 3D [2, 3].

Concerning the chemical process, principal aerosol precursors (unburned hydrocarbons (UHCs), particles, nitrogen oxides, sulfur oxides) will be interested. [4].

Firstly, the aircrafts produce 35% of total emissions of UHCs in the world [5]. That is why the study of the production of UHCs is required. Secondly, particulate matter (PM for Particulate Matters) is emitted by aircraft engines, these include organic soluble fraction and the insoluble fraction consisting mainly soot. Soot is a chemical compound issued from the incomplete combustion of fossil fuels (gasolines, diesels, fuel oils, kerosene, carbons) or biomass (wood, plants)[6]. In the exhaust gas, the soot is present in a particulate state with a diameter less than one micrometer [7]. The formation of soot depends strongly on the variation of the temperature and the dilution ratio [6]. The evolution of soot particles also depends on the amount of oxygen in the post-combustion zone (HPT) which favors the oxidation of the latter. Few articles deal with soot particles and their evolution in the turbine and will be performing as part of this study. Thirdly, analysis of nitrogen oxides generated by the combustion is often studied because it is regulated by international instances. Indeed, the nitrogen oxides are mainly quantified by the warning and measuring air pollution networks. The family of nitrogen oxides comprises the following compounds: nitrogen monoxide (NO),

nitrogen dioxide (NO_2), nitrogen protoxide (N_2O), dinitrogen tetroxide (N_2O_4) trioxide nitrogen (N_2O_3). Among them, the most important are NO and NO_2 namely NO_x, they are two odorous and toxic gases even at low doses and the irritation of the mucous begins as soon as the content (by volume) than 0.0013%. The oxidation of nitrogen (in air) occurs at high temperatures and creates NO_x [4, 5]. Today, NO_x are emitted in large quantities by transport and industry. The NOx modeling was performed by Lukachko [3] and their evolution depends on the residence time and the position in the turbine. Based on these results, the authors show that the concentration of NOx is quite stable in the turbine.In this study, we will use the data in the literature as initial conditions and then modeled in 3D of NO_x formation in each zone of the HPT. Finally, concerning the sulfur oxides, there are more than 30 sulfur oxides (S_nO_m) among them only two are important, SO_2 and SO_3 in terms of environmental impact. They participate as precursors to the formation of aerosols and are increasing in the atmosphere due to the increase of air traffic [8]. The combustion of fossil fuels causes the production of 55% of the sulfur dioxide in the atmosphere. The emissions depend on the chemical reactions taking place in the engine [9]. In the literature, measurements and simplified models gave a global emission index: EI (SO_2) de 1.0 g (kg fuel)$^{-1}$. In this study, the detailed calculation of the SO_x contents in the HPT will be effected.

The present work aims to evaluate the influences of different operating conditions on the thermodynamic process and influences of the flow through turbomachinary blades on the chemical transformation process of aerosol precursors (e.g. nitrogen oxides, sulfur species) and to analyze the interactions between the geometrical parameters, thermodynamical and chemical processes including aerosol precursor formation in the turbine. The results obtained in this work have been compared to those developed by using 1D and 2D CFD modeling of the HPT [2, 3, 5, 10, 11].

2. Governing equations

2.1. Fluid dynamic

In this study, the RANS approach (Reynolds – Averaged Navier - Stokes equations) and the k - ε model (two equations) were used to solve governing equations [12, 13]. Where *k* is the turbulence kinetic energy and is defined as the variance of the fluctuations in velocity (m^2/s^2). ε is the turbulence eddy dissipation (the rate at which the velocity fluctuations dissipate), and has dimensions of *k* per unit of time (m^2/s^3).

The governing equations are described below in three dimensions (x, y, z):

$$\frac{\partial \rho}{\partial t} + \frac{\partial}{\partial x_j}(\rho U_j) = 0 \qquad \text{(Eq.1)}$$

$$\frac{\partial \rho U_i}{\partial t} + \frac{\partial}{\partial x_j}(\rho U_i U_j) = -\frac{\partial p}{\partial x_i} + \frac{\partial}{\partial x_j}\left(\tau_{ij} - \rho\overline{u_i u_j}\right) + S_M \qquad \text{(Eq.2)}$$

where in a Cartesian co-ordinate system, the velocity component u_i can be replaced by the sum of a mean and fluctuating component $u_i = U_i + u_i'$; S_M is source term of the rotor speed, τ is the molecular stress tensor (including both normal and shear components of the stress)[12].

The *k-ε* model introduces two new variables into the system of equations. The values of *k* - *ε* come directly from the differential transport equations for the turbulence kinetic energy and turbulence dissipation rate. ANSYS FLUENT solves the energy equation in the following form:

$$\frac{\partial(\rho k)}{\partial t} + \frac{\partial}{\partial x_j}(\rho U_j k) = \frac{\partial}{\partial x_j}\left[\left(\mu + \frac{\mu_t}{\sigma_k}\right)\frac{\partial k}{\partial x_j}\right] + P_k - \rho\varepsilon + P_{kb} + S_h \qquad \text{(Eq.3)}$$

where S_h is the energy source term due to chemical reaction computed as :

$$S_h = -\sum_j \frac{h_j^{\,o}}{M_j}\mathbb{R}_j \qquad \text{(Eq.4)}$$

where $h_j^{\,o}$ is the enthalpy of formation of species j and $\mathbb{R}_j$ is the volumetric rate of creation of species j [12].

Two-equation turbulence models are widely used, due to a good compromise between numerical effort and computational accuracy.

2.2. Chemical modeling

Calculations with chemical reactions were also carried out with a chemical kinetic including about 35 species and 110 reactions (described in [3, 11, 14, 15]) where low and medium pressure are taken into account.

Concerning the changes of the NO_x, those changes are often described by two mechanisms: Zeldovich mechanism (at very high temperatures - thermal NO_x mechanism) and Fenimore mechanism (at lower temperatures - prompt NO_x mechanism) [12, 16]

Concerning the changes of the SO_x, a detailed sulfur oxidation reaction mechanism was proposed by Kramlich [17]. The mechanism consists of 20 reversible reactions and includes 12 species (S, S_2, SH, SO, SO_2, H_2S, H, H_2, OH, H_2O, O_2 and O). Subsequently, this mechanism has been reduced to 8 steps and 10 species (with the removal of S and S_2) because the formation of SO_3 is small and negligible in the sulfur oxidation reaction.

The presence of soot in the HPT mainly issued from the incomplete combustion of hydrocarbons. The structure of soot has two forms: simple and condensed [12]. The simple form occurs at temperatures above 873 K which is joint preliminary layers of globular form and each globular form comprises between 105 to 106 carbon atoms. Condensed form appears at temperatures below 873 K. This soot is covered by heavy organic compounds: unburned hydrocarbons, ketone, ester, organic acids. This form represents from 50% to 80% of the total soot according to the aircraft engine type [12].

3. Computational setup

3.1. Rotor and stator design

Firstly, the rotor and stator geometry of type engine CFM56 was built by BLADE GEN. Regarding the stator, the geometrical dimensions are entered. Next, the construction of the blade surface is performed.

The main angles (horizontal angle of blade profile - theta and vertical angle of blade profile - Beta) are also implemented. More specifically, the theta function according to the stator blade positions was represented in Fig. 1.

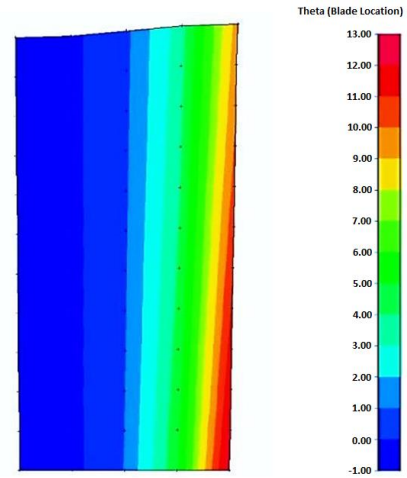

Fig. 1. The theta function according to the stator blade positions

To continue to define the blade geometry, half of blade thickness as a function of cord percentage was defined. With the length of cord (C) is to 71.7131 and the ratio of cord (S/C) is to 0.517543, the stator blade profile was obtained.

The choice of the stator blade dimensions allows obtaining the profile of stator body where $R_{in\ stator}$ = 254 mm, $R_{outi\ stator}$ = 356.0 mm, $R_{oute\ stator}$ = 360 mm and $R_{in\ stator}$, $R_{outi\ stator}$, $R_{oute\ stator}$ are respectively inside, entered outside and exited outside radius of the stator body. For an engine CFM56 type, the number of stator blades of HPT is equal to about 43. It can be found the stator profile structure of total.

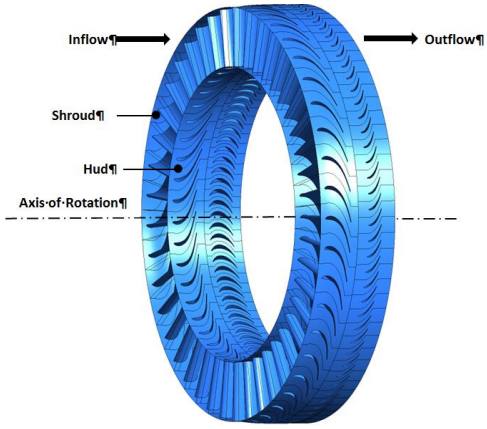

Fig. 2. The complete structure of the HPT

Repeat the process, with $R_{in\ rotor}$ = 254 mm, $R_{outi\ rotor}$ = 360 mm and $R_{oute\ rotor}$ = 360mm (respectively inside, entered outside and exited outside radius of the rotor body) and the number of rotor blades of HPT is equal

to about 83, the rotor blade profile and the rotor profile structure of total are also obtained.

Then, performing of the assembly of stator and rotor helps to obtain the complete structure of the HPT as shown in Fig. 2.

The mesh system was then established with about 5,000,000 elements. To simplify the calculation, the periodic boundary conditions were imposed on the surfaces of a block of stator blade fluid domain and rotor blade fluid domain. It is necessary to couple the outlet of the stator blade fluid domain to that associated to the rotor blade inlet.

3.2. Thermodynamical and chemical conditions

Table 1. Chemical species at the combustion chamber outlet [2, 3]

Composants	ppmv	Mole fraction
NO	130	0.002515732
NO_2	14.5	0.000280601
NO_3	0.0000432	8.35997E-10
HNO	0.012	2.32221E-07
HNO_2	0.14	2.70925E-06
HNO_3	0.000471	9.11469E-09
N_2O	0	0
SO	0.0000136	2.63184E-10
SO_2	10.6	0.000205129
SO_3	0.332	6.42479E-06
HSO_3	0.0000985	1.90615E-09
H_2SO_4	0.0000209	4.04452E-10
C	5.86	0.000113401
O	1.47	2.84471E-05
O_2	130	0.002515732
OH	60	0.001161107
HO_2	0.831	1.60813E-05
H_2O_2	0.0252	4.87665E-07
H	0.00758	1.46687E-07
H_2	0.249	4.81859E-06
N	0	0
H_20	47.8	0.000925015
CO	201	0.003889708
N_2	772	0.014939576
CO_2	50300	0.973394639

Concerning thermodynamic conditions, the rotor speed was set by SNECMA on an aircraft turbine CFM-56 to 8500 tr/min [10], $P_{in\ stator}$ = 31.13 bar, $V_{in\ stator}$ = 118 m/s and $T_{in\ stator}$ = 1343 K [3] with an initial rate of turbulence at the stator inlet of 5% and 1% at the stator outlet . Where $P_{in\ stator}$, $V_{in\ stator}$, $T_{in\ stator}$ are respectively pressure, velocity and temperature of the stator inlet.

The type of wall treatment implemented herein, has been proposed in [18], is a temperature slip boundary condition.

Concerning chemical conditions, the initial conditions were set, using a user define function, according to the table 1 [2, 3] in order to study the chemical species quantities at the combustion chamber outlet.

More than 6000 iterations according to the positions of HPT are used to solve equations, resulting in high resolution in the both space and time.

4. Results and discussion

4.1 Evolution of thermodynamic changes in the HPT

4.1.1 Evolution of temperature

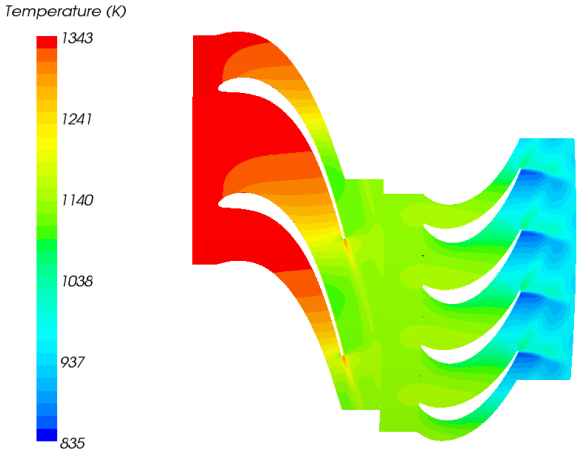

Fig. 3. Evolution of temperature in the HPT

Fig. 3 shows that the temperature gradient decreases in the HPT from 1343 K at the stator inlet to 951 K at the rotor outlet. Its static enthalpy is then converted to kinetic energy. The fluid is accelerated while the temperature decreases in the direction of rotation.
Relative to the moving blades, there is acceleration of the fluid with the associated decrease in static temperature. Further thermal loss causes also the temperature decreases.
Fig. 3 shows also that the non-moving stator and the longer of stator implicated the temperature change in stator is almost constant and there is more important temperature change in the zone near rotor hub. The change of temperature tendency in every rotor zone can attributed by the moving blades and rotor blade profiles. These results are in good agreement with

that reported by Data NASA Lewis Research Center and Elements of gas turbine propulsion of Mattingly [2, 24].

4.1.2 Evolution of pressure

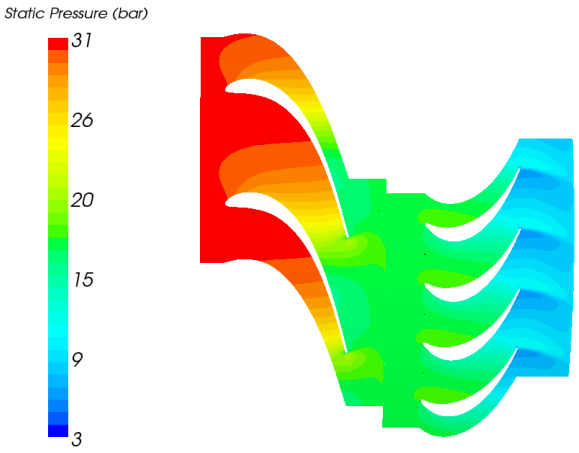

Fig. 4. Evolution of pressure in the HPT

Fig. 4 presents that similar tendency of temperature behavior, the pressure gradient in the HPT also decreases, falling from 30.6 bar at the inlet to 8.8 bar at the outlet. The change of pressure happens at every position of HPT.

The following analysis of the axial – flow turbine is performed along the mean radius with radial variations being considered. There is a variation of pressure from root to tip and the flow pressures are different at each radius. The change of blade profiles has strongly influenced on the pressure evolution among the HPT. Relative to the moving blades, the pressure variations in rotor are more powerful than that in stator.

4.3 Evolution of velocity

Fig. 5 demonstrates the streamlines of velocity and their values in the HPT. These streamlines in the rotor are more turbulent than themselves in the stator caused by the moving rotor blades.

This velocity increases from 112 m/s to 614 m/s and then decreases from 614 m/s to 302 m/s. The velocity gradient has a good agreement from that reported in the Data reported by NASA Lewis Research Center [2]. The velocity gradient in stator is positive because the static enthalpy of temperature is then converted to kinetic energy. So in the stator, the fluid is accelerated while the temperature decreases in the direction of rotation. In the rotor, relative to the moving blades, this influences on the absolute flow velocity and changes their values; also the kinetic energy of the fluid is then converted to kinetic energy of blade associated decrease in flow velocity in rotor.

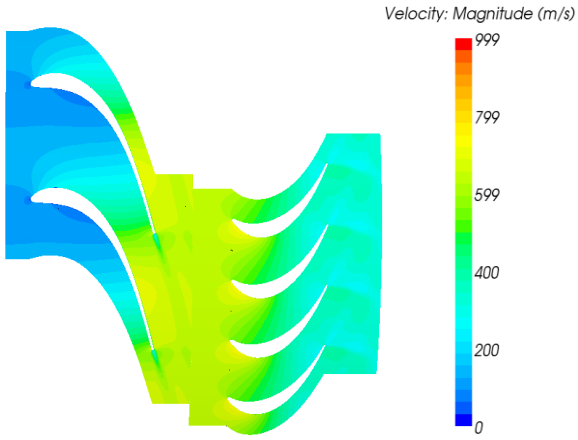

Fig. 5. Evolution of velocity in the HPT

4.2 Influences of different operating conditions

4.2.1 Influences of initial temperature at the stator inlet

The initial temperature effects at the stator inlet are considered depending on the function of engine in four different cases: starting (1329 K), take-off (1554 K), cruise (1341K) and maximum cruise (1519). Fig. 6 shows the temperature evolution of the cutting to 50% of radius of the blades, the profiles in two cases are entirely the same, just difference of value. Concerning the initial temperature 1341 K, the temperature at the rotor output is 959 K and about the initial temperature 1554 K, this value is 1173 K.

More detail, Fig. 7 shows the temperature profile in the extrados of stator blade in the four cases. The temperature value in the HPT is proportional in relation to initial temperature and this value is the biggest in the take-off (1554 K) and the smallest in the starting (1329 K). It has an important significance to study the formation of pollutants in the different temperature zones in the section 4.3 - Evolution of chemical changes in the HPT.

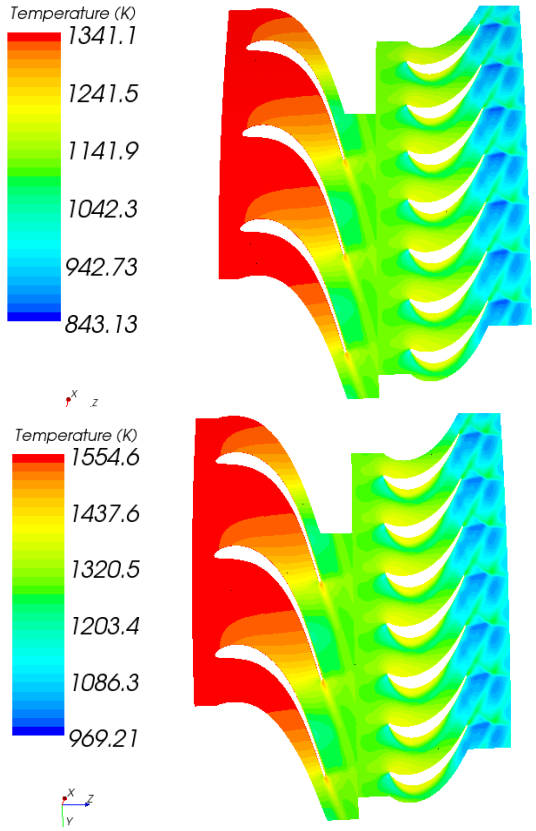

Fig. 6. Evolution of static temperature in two cases of initial temperatures: cruise (1341K) and take - off (1554 K)

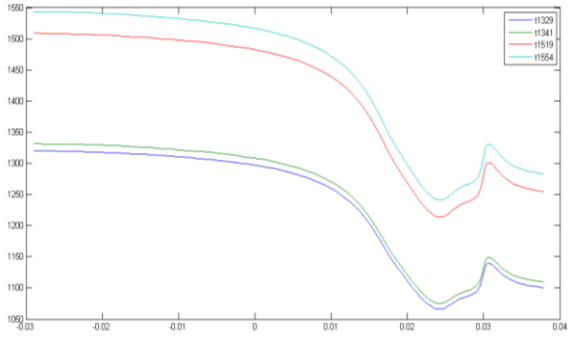

Fig. 7. Temperature profile in the extrados of stator blade in the four cases: starting (1329 K), take-off (1554 K), cruise (1341K) and maximum cruise (1519)

The influences of initial temperatures on the velocity are the same of the temperature (see Fig. 8). The velocity value is the biggest in the take-off (1554 K) and the smallest in the starting (1329 K). This may be explained by the increase of temperature as the rise of potential energy involving increase of kinetic energy or velocity by the transfer of these energies. Oppositely, the influences of the initial temperatures are not strongly on the pressure.

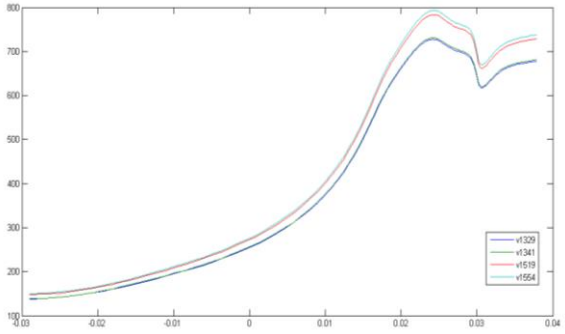

Fig. 8. Velocity profile in the extrados of stator blade in the four cases: starting (1329 K), take-off (1554 K), cruise (1341K) and maximum cruise (1519

Fig. 9 shows the turbulent kinetic energy profile in the four cases. The profiles are the same gradient and this energy is the biggest in the take-off (1554 K) and the smallest in the starting (1329 K) because when the increase of temperature accelerates the fluctuations of velocity components. So the turbulent kinetic energy increases according to the initial temperature rise.

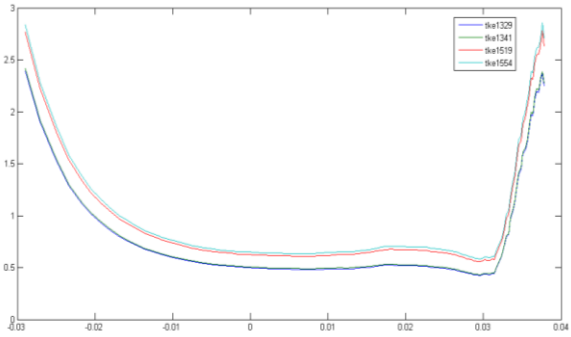

Fig. 9. Turbulent kinetic energy profile in the extrados of stator blade in the four cases: starting (1329 K), take-off (1554 K), cruise (1341K) and maximum cruise (1519

4.2.2 Influences of rotor speed

Fig. 10 shows the temperature profile in the extrados of stator blade when the rotor speed changes in three cases: 8500 tr/min, 12500 tr/min and 15183 tr/min (maximum operating speed). The influences of these speeds on the temperature field are not strongly. The area has the biggest influence in the stator being near the surface of the stator outlet where there is the rotor speed influence. In the same way, the evolutions of pressure and velocity are slightly influenced from the changes of rotor speed (see Fig. 11).

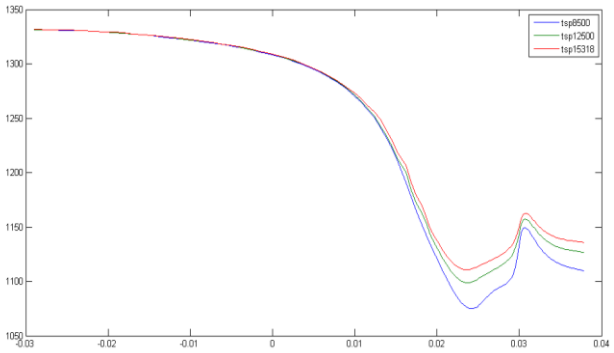

Fig. 10 Temperature profile in the extrados of stator blade in three cases of rotor speed: 8500 tr/min, 12500 tr/min and 15183 tr/min (maximum operating speed)

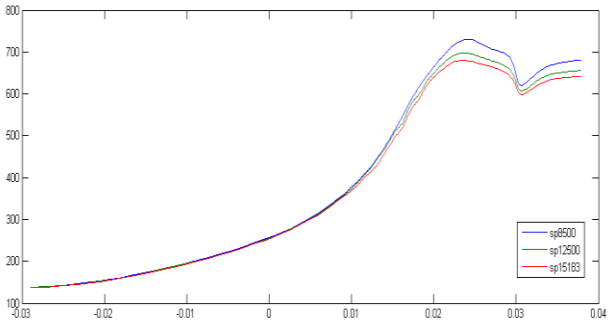

Fig. 11 Velocity profile in the extrados of stator blade in three cases of rotor speed: 8500 tr/min, 12500 tr/min and 15183 tr/min (maximum operating speed)

Fig. 12 illustrates the turbulent kinetic energy evolution of the cutting to 5% of radius of the blades in two cases of rotor speeds: 8500 tr/min and 15183 tr/min (maximum operating speed). The energy extends longer at the end of stator blade in the case 15183 tr/min. By cons, the turbulent zone in the extrados of rotor blade is shrank in the case 15183 tr/ min by the rotor speed influences. These influences also implies directly and strongly on the velocity field especially in the area around the extrados of the rotor blades and the contact area between stator and rotor.

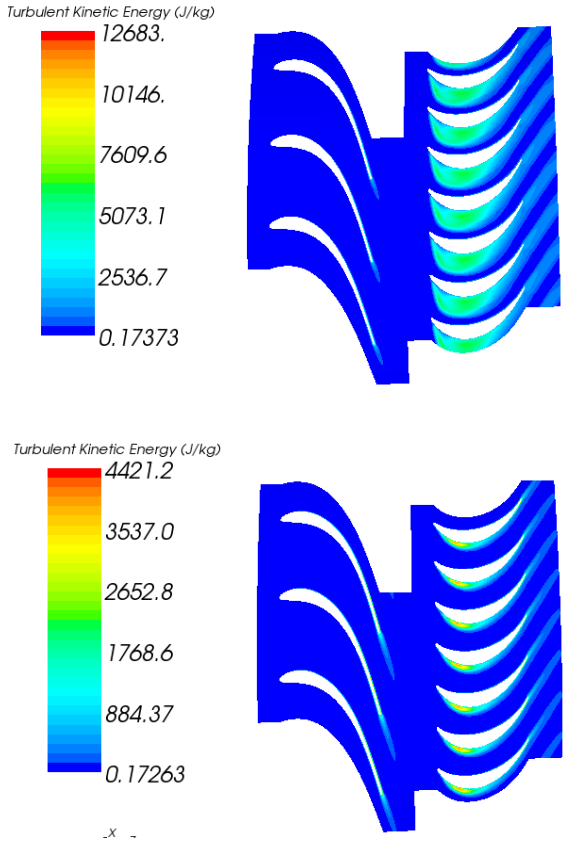

Fig. 12 Turbulent kinetic energy evolution in the HPT in two cases of rotor speed: 8500 tr/min and 15183 tr/min (maximum operating speed)

4.3 Evolution of chemical changes

Calculations with chemical reactions were also carried out with a chemical kinetic including about 35 species and 110 reactions (discussed in [3, 11, 14, 15, 19-21]) where low and medium pressure are taken into account.

In following section, the evolution of pollutants such as NO_x, SO_x, H_2S and soot particles will be described.

1. Evolution of the NO_x

The changes of the NO_x is often described by two mechanisms: Zeldovich and Fenimore mechanisms [12, 16]. From these mechanisms at different temperatures, the evolution of NO_x can be determinate.

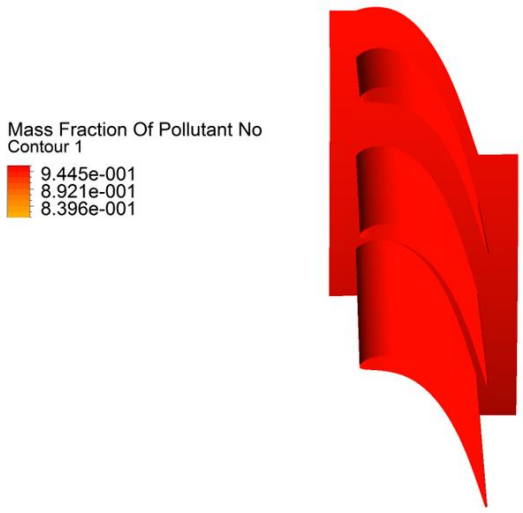

Fig. 13. Contour of the mass fraction of the NO_x (dominated by NO) in the HPT

Fig. 13 shows that in the stator, the NO_x contains about 96.2% of calculated total pollutant species weigh (SO_x and particles). At the turbine HPT outlet, the quantity of NO_x reached a value of 4.81% of the total weight of all products (also including pollutants).

It also shows that the mass fraction of NO_x remains stable and therefore very little change in the range of temperatures of the HPT. Farokhi (2014) demonstrates that both types of oxides of nitrogen NO and NO_2 at temperature under 1800 K are majority referred to as NO_x of turbine emission [22]. But the stability of NO_x emission mainly depends on NO emission which is dominant compared to NO_2 (the unstable compound) [12, 23].

2. Evolution of the SO_x and H_2S

As describing in the previous sections, there are more than 30 sulfur oxides (S_nO_m) but there are only SO_2 and SO_3 that have the most negative environmental impact. However, the formation of SO_3 is often small and negligible. So we concentrated the evolution of SO_2.

Concerning the changes of the SO_x, a detailed sulfur oxidation reaction mechanism was proposed by Kramlich [17]. This mechanism consists of 20 reversible reactions and includes 12 species (S, S_2, SH, SO, SO_2, H_2S, H, H_2, OH, H_2O, O_2 and O). Subsequently, this mechanism has been reduced to 8 steps and 10 species (with the removal of S and S_2).The evolution of the SO_x and H_2S are identified and described in Fig. 14 and Fig. 16.

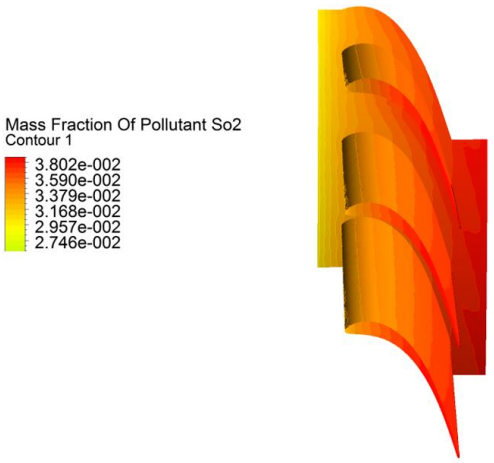

Fig. 14. Contour of the mass fraction of SOx (SO2) in the HPT

Fig. 14 shows that the mass fraction of SO_x compared to other pollutant species increased from 2.71% at the stator inlet to 3.87% at the stator outlet. Finally, SO_x at the HPT outlet represents only 0.1936% of the total mass of all species produced.

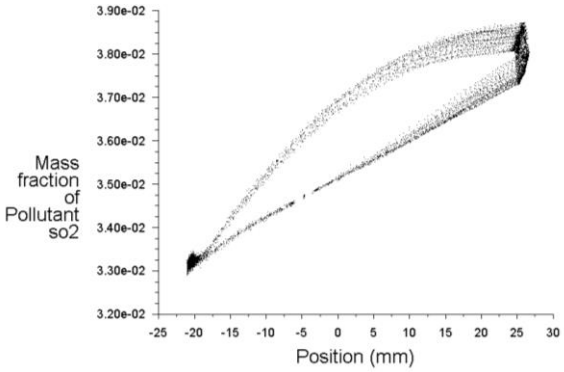

Fig. 15. Contour of the mass fraction of SOx (SO2) among the axe z (the direction of flow) of the stator blade in the HPT

In detail, Fig. 15 shows the change of SO_x in intrados and extrados of stator among the axe z (the direction of flow). The values of SO_x in extrados are bigger than them in intrados and generally gradient orientation is positive in the both intrados and extrados causing by the production reactions of SO_2.

Fig. 16 demonstrates that the H_2S gas decreases from 0.5% to 0.075% by total mass of pollutants in the stator. The compound at the HPT outlet represents of 0.025% of total mass of all species produced. The decrease of H_2S in the stator is directly related to the production of SO_x. In more detail, Fig. 17 shows contour of the mass fraction of H2S among the axe z

(the direction of flow) of the stator blade. It is noted that like the evolution of SO_x, the values of H_2S in extrados is always bigger than them in stator blade intrados. But oppositely with the change of SO_x, the gradient of H_2S is negative. The loss of H_2S is directly linked with the increase of SO_x.

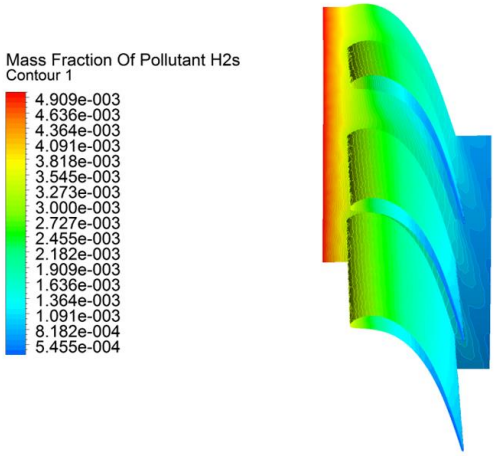

Fig. 16. Contour of the mass fraction of H2S in the HPT

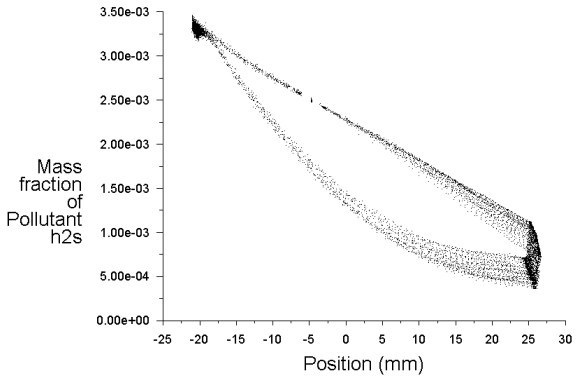

Fig. 17. Contour of the mass fraction of H_2S among the axe z (the direction of flow)of the stator blade in the HPT

3. Evolution of soot

The formation of soot particles and their oxidation in the HPT is a very complex process [7]. The soot is produced mainly in the fuel-rich regions of the primary zone in the combustor. Soot particles are primarily carbon (96% by weight), hydrogen and some oxygen [22]. Soot particles are strongly influenced by the temperature profile which depends on the structure of the flow and mixing in the primary zone [7, 22].

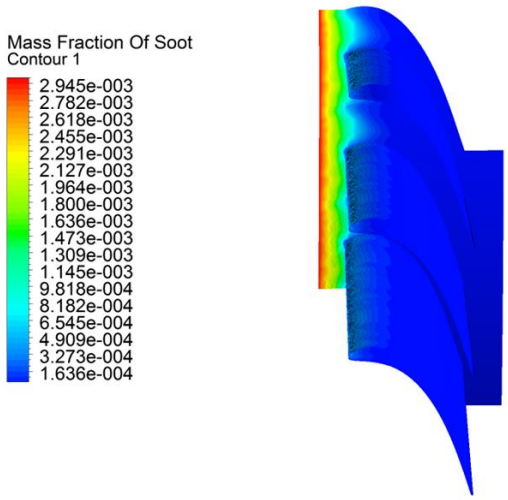

Fig. 18. Contour of the mass fraction of the soot in the HPT

Fig.18 indicates that the fraction mass of soot particles decreases among the axe of rotation. This represents at the HPT inlet about 0.3 % of total mass of pollutants and decreases to 0.015 % at the HPT outlet.

This decrease is related to the reduction of unburned hydrocarbons which is a component part of soot along the HPT. Also, the structure of blade profiles of stator and rotor and the moving blades of rotor increase the dilution zones which cause the decrease of the fuel – rich regions and finally the decrease of soot particles. Moreover, these results can be explained by a reduction of temperature and condensed soot at the zones below 873 K and thus the total mass of soot is lower. These obtained results are completely agree with the research published by Sorokin [7] and Farokhi [22].

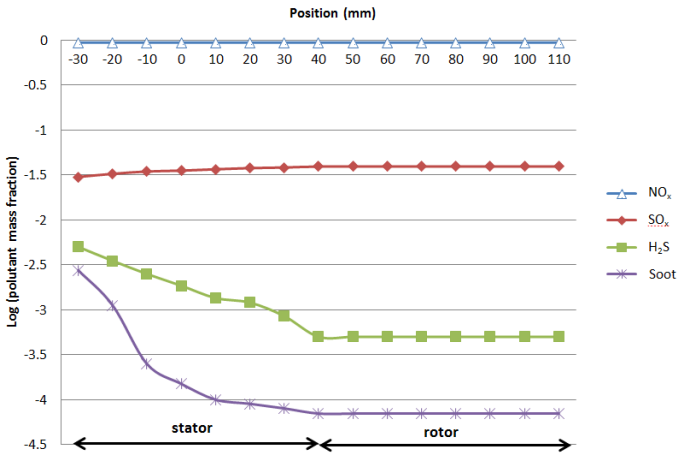

Fig. 19. Graphic of the pollutant mass fraction of the NOx, SOx, H2S et soot according the positions in the HPT

In summary, Fig. 19 shows the graphic of the pollutant mass fraction of the NO_x, SO_x, H_2S in the HPT. It can be seen from this figure that the major pollutants are NO_x following by SO_x and soot. The emissions of NO_x are almost stable but the H_2S emission strongly decreases in the HPT. This can be linked to the increasing of SO_x. Concerning the soot particles, we can see the decrease of soot among the HPT and the soot particles occupy a small amount in the quantity of total pollutants.

4 Conclutions

3D-Modeling and simulation of thermodynamic transformations and chemical processes of an aircraft engine turbine with the different operating conditions and the relationship between the geometrical parameters, thermodynamic and chemical processes including aerosol precursor formation (NO_x, SO_x and soot) are investigated.

This model has been successfully used to evaluate the evolution of the pollutant gases emission in an aircraft engine turbine. It was found that the formation of pollutants gases in HPT is a complex process depending on several factors including the HPT geometry, the evolution of the flow, the temperature and the chemical reactions. By using the 3D-modelling and simulation (ANSYS) and chemical species at the combustion chamber outlet in the literature, our finding shows that the mass fractions of NO_x, SO_x, H_2S and soot to the total mass of the pollutant species are respectively 96.2%, 3.87%, 0.075% and 0.15%. These results have a good agreement the literature [2, 5-7, 22, 24, 25]. This work provides the useful information to better understand of the thermodynamic and chemical processes occurs in the turbine and may be help to develop technologies to reduce the pollution gases for environment in the future.

References

1. Gagnepain, L., *Les véhicules légers: bilan des filières*, 2005.
2. Starik, A.M., et al., *Modeling of sulfur gases and chemiions in aircraft engines.* Aerospace Science and Technology, 2002. **6**(1): p. 63-81.
3. Lukachko, S.P., et al., *Production of sulfate aerosol precursors in the turbine and exhaust nozzle of an aircraft engine.* Journal of Geophysical Research-Atmospheres, 1998. **103**(D13): p. 16159-16174.
4. Jones, R.E., *Gas turbine engine emissions—Problems, progress and future.* Progress in Energy and Combustion Science, 1978. **4**(2): p. 73-113.
5. Mogilka, P., *Contexte, enjeux, progrès accomplis et perspectives pour l'avionneur*, 2011.
6. Wong, H.W., et al., *Design Parameters for an Aircraft Engine Exit Plane Particle Sampling System.* Journal of Engineering for Gas Turbines and Power-Transactions of the Asme, 2011. **133**(2).
7. Sorokin, A., X. Vancassel, and P. Mirabel, *Emission of ions and charged soot particles by aircraft engines.* Atmospheric Chemistry and Physics, 2003. **3**: p. 325-334.
8. Hofmann, D.J., *Aircraft Sulfur Emissions.* Nature, 1991. **349**(6311): p. 659-659.
9. Brown, J., *Ten years of robotics and laboratory automation in a production control laboratory.* Proceedings of the International Symposium on Laboratory Automation and Robotics 1996, 1997: p. 688-688.
10. EASA, *Type – Certificate Data Sheet*, 2006.
11. Tsang, W. and J.T. Herron, *Chemical Kinetic Data-Base for Propellant Combustion .1. Reactions Involving No, No2, Hno, Hno2, Hcn and N2o.* Journal of Physical and Chemical Reference Data, 1991. **20**(4): p. 609-663.
12. Fluent. Ansys, I., 2011.
13. Versteeg, H.K. and W. Malalasekera, *An introduction to computational fluid dynamics: the finite volume method*2007: Pearson Education.
14. Yetter, R.A., et al., *Development of Gas-Phase Reaction-Mechanisms for Nitramine Combustion.* Journal of Propulsion and Power, 1995. **11**(4): p. 683-697.
15. Hsu, K.J. and W.B. Demore, *Rate Constants for the Reactions of Oh with Ch3cl, Ch2cl2, Chcl3, and Ch3br.* Geophysical Research Letters, 1994. **21**(9): p. 805-808.
16. Fenimore, C.P., *"Formation of Nitric Oxide in Premixed Hydrocarbon Flames".* In 13th Symp.(Int'l.)on Combustion. The Combustion Institute. 373., 1971.
17. Kramlich, J.C., *"The Fate and Behavior of Fuel-Sulfur in Combustion Systems", thesis*, 1980, Washington State University.
18. Goldstein, M.a.J.R.H., *"Boundary Conditions for the Diffusion Solution of Coupled Conduction-Radiation Problems"*, in *NASA Technical Note, NASA TN D-4618.*
19. Westley, F., J. Herron, and R. Cvetanovic, *Compilation of chemical kinetic data for combustion chemistry. Part 2. Non-aromatic C, H, O, N, and S containing compounds (1983)*, 1987, National Bureau of Standards, Washington, DC (USA). Chemical Kinetics Div.
20. Tsang, W. and R. Hampson, *Chemical kinetic data base for combustion chemistry. Part I. Methane and related compounds.* Journal of Physical

and Chemical Reference Data, 1986. **15**(3): p. 1087-1279.
21. DeMore, W.B., et al., *Chemical kinetics and photochemical data for use in stratospheric modeling. evaluation no. 12.* 1997.
22. Farokhi, S., *Aircraft propulsion*2014: John Wiley & Sons.
23. Cumpsty, N.A., *Jet Propulsion: A simple guide to the aerodynamic and thermodynamic design and performance of jet engines*. Vol. 2. 2003: Cambridge University Press.
24. Schumann, U., *The impact of NOX emissions from aircraft upon the atmosphere at flight altitudes 8–15 km (AERONOX).* CEC Report, 1995.
25. Barnes, F., et al., *NOx emissions from radiant gas burners.* Journal of the Institute of Energy, 1988. **61**(449): p. 184-188.